Appl. Math. Mech. -Engl. Ed., 2008, **29**(8):1093–1104
DOI 10.1007/s10483-008-0813-x

Applied Mathematics and Mechanics (English Edition)

Influence of magnetic field and Hall currents on blood flow through a stenotic artery *

Kh. S. Mekheimer[1], M. A. El Kot[2]

(1. Department of Mathematics, Faculty of Science, Al-Azhar University, Nasr City 11884, Cairo, Egypt;
2. Department of Mathematics, Faculty of Education, Suez Canal University, Suez, Egypt)

(Communicated by ZHOU Zhe-wei)

Abstract A micropolar model for blood simulating magnetohydrodynamic flow through a horizontally nonsymmetric but vertically symmetric artery with a mild stenosis is presented. To estimate the effect of the stenosis shape, a suitable geometry has been considered such that the horizontal shape of the stenosis can easily be changed just by varying a parameter referred to as the shape parameter. Flow parameters, such as velocity, the resistance to flow (the resistance impedance), the wall shear stress distribution in the stenotic region, and its magnitude at the maximum height of the stenosis (stenosis throat), have been computed for different shape parameters, the Hartmann number and the Hall parameter. This shows that the resistance to flow decreases with the increasing values of the parameter determining the stenosis shape and the Hall parameter, while it increases with the increasing Hartmann number. The wall shear stress and the shearing stress on the wall at the maximum height of the stenosis possess an inverse characteristic to the resistance to flow with respect to any given value of the Hartmann number and the Hall parameter. Finally, the effect of the Hartmann number and the Hall parameter on the horizontal velocity is examined.

Key words stenotic artery, Hall currents, blood flow

Chinese Library Classification 76Z05, 92C10
2000 Mathematics Subject Classification O361.3, O361.4, Q66

Introduction

Arteriosclerosis is a common disease which severely influences human health. Early arteriosclerotic lesions are not randomly distributed throughout the arterial tree, they usually tend to form and grow at certain locations, such as the distal to abdominal aorta, coronary arteries and carotid bifurcations. It has been found that the initiation and localization of arteriosclerosis is closely related to local hemodynamic factors (such as wall shear stress, etc.). Stenosis in the arteries of mammals is a common occurrence. For many years, researchers have endeavored to model the flow of blood through the stenosed arteries both experimentally and theoretically. This is an important field of study, as arterial diseases are a chief cause of death in most of the western world. Although the genesis of such diseases remains unknown, there is a strong

* Received Mar. 22, 2007 / Revised Jun. 6, 2008
Corresponding author Kh. S. Mekheimer, Ass. Prof., Doctor, E-mail: kh-mekheimer@yahoo.com

belief that hydrodynamic factors play a very significant role in the formation and proliferation of the disease. It is well known that seventy five percent of all deaths are caused by circulatory disorders. The deposition of cholesterol and proliferation of the connective tissues in the arterial wall form plaques which grow inward and restrict blood flow. Stenosis or arteriosclerosis, which means narrowing of any body passage (tube or orifice), is thus an abnormal and unnatural increase in the arterial wall thickness that develops at various locations of the cardiovascular system under diseased conditions.

If a magnetic field is applied to a moving and electrically conducting liquid, it will induce electric and magnetic fields. The interaction of these fields produces a body force known as the Lorentz force, which has a tendency to oppose the movement of the liquid[1]. Stud et al.[2] studied the effect of a moving magnetic field on blood flow, and observed that the effect of a suitable moving magnetic field accelerates the speed of blood. Agrawal and Anwaruddin[3] studied the effect of a magnetic field on blood flow by taking a simple mathematical model for blood through an equally-branched channel with flexible walls, which execute peristaltic waves using a long wave-length approximation method. They observed that, for the flow of blood in arteries with arterial diseases like arterial stenosis or arteriosclerosis, the influence of a magnetic field may be utilized as a blood pump in carrying out cardiac operations. When the conducting fluid is an ionised gas, or the strength of the applied magnetic field is very large, the conductivity normal to the magnetic field is reduced due to the free spiraling of electrons and ions about the magnetic lines of force before suffering collisions; and a current is induced in a direction normal to both electric and magnetic fields. This phenomenon is called the Hall effect.

Bharali and Borkakati[4] studied the effect of the Hall currents on the magnetohydrodynamic (MHD) flow of an incompressible, viscous and electrically conducting fluid between two nonconducting porous plates in the presence of a strong uniform magnetic field. Asghar et al.[5] studied the influence of the Hall currents on the unsteady hydromagnetic flows of an oldroyed-B-fluid. Megahed et al.[6] investigated the effects of heat and mass transfer along a semi-infinite vertical flat plate under the combined buoyancy force of thermal and species diffusion in the presence of a strong non-uniform magnetic field and the Hall currents. Mohyuddin and Ashraf[7] obtained certain forms of the stream function inverse solutions of an incompressible viscoelastic fluid for a porous medium channel in the presence of the Hall currents. Hayat et al.[8] studied the effects of the Hall currents on an unsteady duct flow of a non-Newtonian fluid in a porous medium. Hayat et al.[9] investigated the influence of the Hall currents on the unsteady hydromagnetic oscillatory flow of a second-grade fluid (non-Newtonian fluid).

The theory of micropolar fluids due to Eringen[10] is a subclass of microfluids. In the micropolar theory, a part of the classical velocity field, the microrotation vector and the gyration parameter are introduced to investigate the kinematics of microrotations. The micropolar fluid, such as liquid crystals, suspensions and animal blood, etc., consists of randomly oriented bar-like elements or dumbbell molecules. In addition to the translatory motion in an average sense, each volume element has a microrotation about its centroid. The micropolar fluid theory deviates from the classical Navier-Stokes model of viscous fluid, regarding the suspenance of couple stress in the fluid and the non symmetry of the stress tensor. The model of micropolar fluid takes account of the fact that fluid particles contained in a small volume element, besides following the rigid body rotation of the volume element, can rotate about the centroid of the volume element[11]. Although blood is a good conductor of electricity, a number of researchers have studied the flow of blood through stenosed arteries in the absence of a magnetic field[12−23]. In this paper, we study the effect of a magnetic field and the Hall currents on a micropolar fluid (as a blood model) through an artery with a mild stenosis. Such analysis may be useful in understanding the magnetic resonance angiography, which is one of radiological investigations done for atherosclerosis.

1 Analysis

The equations, which govern the steady flow of an incompressible micropolar and electrically conducting fluid of constant viscosity μ and density ρ in the presence of a magnetic field and in the absence of body force and body couple, are

$$\nabla \cdot \boldsymbol{V} = 0, \tag{1}$$

$$\rho(\boldsymbol{V} \cdot \nabla \boldsymbol{V}) = -\nabla p + \kappa \nabla \times \boldsymbol{w} + (\mu + \kappa)\nabla^2 \boldsymbol{V} + \boldsymbol{J} \times \boldsymbol{B}, \tag{2}$$

$$\rho j(\boldsymbol{V} \cdot \nabla \boldsymbol{w}) = -2\kappa \boldsymbol{w} + \kappa \nabla \times \boldsymbol{V} - \gamma(\nabla \times \nabla \times \boldsymbol{w}) + (\alpha + \beta + \gamma)\nabla(\nabla \cdot \boldsymbol{w}), \tag{3}$$

$$\nabla \times \boldsymbol{B} = \mu_{\mathrm{e}} \boldsymbol{J}, \quad \nabla \cdot \boldsymbol{B} = 0, \quad \nabla \times \boldsymbol{E} = 0, \quad \nabla \cdot \boldsymbol{J} = 0. \tag{4}$$

The generalized Ohm's law taking the Hall effects into account is

$$\boldsymbol{J} = \sigma[\boldsymbol{E} + \boldsymbol{V} \times \boldsymbol{B}] - \frac{\sigma}{e n_{\mathrm{e}}} \boldsymbol{J} \times \boldsymbol{B}. \tag{5}$$

In writing Eq. (5), the ion slip and the thermo-electric effects are neglected. Here $\boldsymbol{B}$ is the total magnetic induction vector; $\boldsymbol{V}$ is the velocity vector; $\boldsymbol{w}$ is the microrotation vector; $\boldsymbol{E}$ is the electric field vector; $\boldsymbol{J}$ is the current density vector; σ is the electrical conductivity of the fluid; e is the electric charge; n_{e} is the number density of electrons; μ_{e} is the magnetic permeability, and j is the microgyration parameter. Furthermore, the material constants (new viscosities of the micropolar fluid) μ, k, α, β, and γ satisfy the following inequalities[10]:

$$2\mu + k \geq 0, \quad k \geq 0; \quad 3\alpha + \beta + \gamma \geq 0, \quad \gamma \geq |\beta|. \tag{6}$$

2 Formulation of the problem

It is assumed that blood flow is represented by an incompressible micropolar fluid of constant viscosity μ and density ρ. Consider the two-dimensional steady hydromagnetic flow of incompressible micropolar fluid in a channel of width $2d_0$ bounded by two walls. Let x- and y-axes be chosen along and perpendicular to the walls, respectively. A uniform magnetic field B_0 is acting along the z- axis (i.e., B_0 is applied in a direction perpendicular to the flow of the fluid). Let u and v be the longitudinal and transverse velocities, respectively. We assume that the flow of blood in the channel with mild stenosis and the geometry of the stenosis, which is assumed to be symmetric, can be described as[12]

$$h(x) = \begin{cases} d_0[1 - \eta(b^{n-1}(x-a) - (x-a)^n)], & a \leq x \leq a+b; \\ d_0, \quad \text{otherwise}, \end{cases} \tag{7}$$

where $h(x)$ and d_0 are the widths of the channel with and without stenosis, respectively. b is the length of the stenosis; $n(\geq 2)$ is a parameter determining the shape of the constriction profile and referred to as the shape parameter (the symmetric stenosis occurs for $n = 2$); L is the length of the channel and a indicates its location (as shown in Fig. 1).

The parameter η is given by

$$\eta = \frac{\delta}{d_0 b^n} \frac{n^{n/(n-1)}}{(n-1)}, \tag{8}$$

where δ denotes the maximum height of the stenosis located at $x = a + \frac{b}{n^{1/(n-1)}}$.

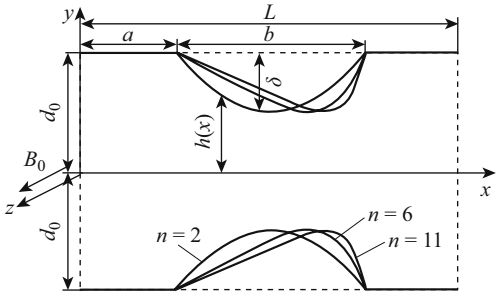

Fig. 1 Geometry of the stenosed channel

The equations governing the problem are

$$\frac{\partial u}{\partial x}+\frac{\partial v}{\partial y}=0, \tag{9}$$

$$\rho\left(u\frac{\partial u}{\partial x}+v\frac{\partial u}{\partial y}\right)=-\frac{\partial p}{\partial x}+(\mu+\kappa)\left(\frac{\partial^2 u}{\partial x^2}+\frac{\partial^2 u}{\partial y^2}\right)+\kappa\frac{\partial \nu}{\partial y}-\sigma B_0^2\alpha(u-sv), \tag{10}$$

$$\rho\left(u\frac{\partial v}{\partial x}+v\frac{\partial v}{\partial y}\right)=-\frac{\partial p}{\partial y}+(\mu+\kappa)\left(\frac{\partial^2 v}{\partial x^2}+\frac{\partial^2 v}{\partial y^2}\right)-\kappa\frac{\partial \nu}{\partial x}-\sigma B_0^2\alpha(v-su), \tag{11}$$

$$\rho j\left(u\frac{\partial \nu}{\partial x}+v\frac{\partial \nu}{\partial y}\right)=-2\kappa\nu-\kappa\left(\frac{\partial v}{\partial x}-\frac{\partial u}{\partial y}\right)+\gamma\left(\frac{\partial^2 \nu}{\partial x^2}+\frac{\partial^2 \nu}{\partial y^2}\right), \tag{12}$$

where p is the fluid pressure, the velocity vector $\boldsymbol{V}=(u,v,0)$, the microrotation vector $\boldsymbol{w}=(0,0,\nu)$. The boundary conditions are

$$u=0,\quad \nu=0\quad \text{at}\quad y=\pm h(x). \tag{13}$$

Introduce the following nondimensional variables

$$\begin{cases} x'=\frac{x}{b}, & r'=\frac{r}{d_0}, & u'=\frac{u}{u_0}, & v'=\frac{bv}{u_0\delta}, \\ h'=\frac{h}{d_0}, & p'=\frac{d_0^2 p}{u_0 b\mu}, & j'=\frac{j}{d_0^2}, & \nu=\frac{d_0\nu}{u_0} \end{cases} \tag{14}$$

into Eqs. (9)–(13) and drop the dashes. By using the assumption, we know that the variation of all the flow characteristics along the axial direction is negligible[17]. The appropriate equations describing the steady flow of a micropolar fluid in the case of a mild stenosis ($\frac{\delta}{d_0}\ll 1$), subject to the additional conditions[16,24]:

(i) $$R_{\mathrm{e}}\frac{\delta n^{\frac{1}{n-1}}}{b}\ll 1, \tag{15}$$

(ii) $$\frac{d_0 n^{\frac{1}{n-1}}}{b}\sim O(1), \tag{16}$$

may be written as

$$\frac{\partial p}{\partial x}=\frac{1}{1-N}\left\{\frac{\partial^2 u}{\partial y^2}+N\frac{\partial \nu}{\partial y}\right\}-H^2\alpha u, \tag{17}$$

$$\frac{\partial p}{\partial y}=0, \tag{18}$$

$$2\nu=-\frac{\partial u}{\partial y}+\frac{2-N}{m^2}\frac{\partial^2 \nu}{\partial y^2}, \tag{19}$$

where u_0 is the velocity averaged over the section of the channel of width d_0, R_e is the channel Reynolds number; $N = \frac{k}{(\mu+k)}$ is the coupling number ($0 \leq N < 1$) (particle size effect parameter), and $m^2 = \frac{d_0^2 k(2\mu+k)}{\gamma(\mu+k)}$ is the micropolar parameter (micropolar spin parameter); $H = \sqrt{\frac{\sigma}{\mu}} B_0 d_0$ is the Hartmann number (suitably greater than $\sqrt{2}$), $\alpha = \frac{1}{1+s^2}$, and $s = \frac{\sigma B_0}{e n_e}$ is the Hall parameter. The corresponding boundary conditions are

$$u = 0, \quad \nu = 0 \quad \text{at} \quad y = \pm h(x),$$

where

$$h(x) = 1 - \eta_1((x-\phi) - (x-\phi)^n), \quad \phi \leq x \leq \phi + 1, \tag{20}$$

here

$$\eta_1 = \frac{\delta^* n^{n/(n-1)}}{(n-1)}, \quad \delta^* = \frac{\delta}{d_0}, \quad \phi = \frac{a}{b}. \tag{21}$$

Differentiating Eq. (19) w. r. t y and adding with Eq. (17), we get

$$u = \frac{1}{(1-N)H^2\alpha}\Big\{\frac{(2-N)}{m^2}\frac{\partial^3\nu}{\partial y^3} - (2-N)\frac{\partial \nu}{\partial y} - (1-N)\frac{\partial p}{\partial x}\Big\}. \tag{22}$$

Substituting Eq. (22) into Eq. (19), we get

$$\frac{\partial^4\nu}{\partial y^4} - \{(1-N)H^2\alpha + m^2\}\frac{\partial^2\nu}{\partial y^2} + \frac{2m^2(1-N)H^2\alpha}{(2-N)}\nu = 0. \tag{23}$$

The general solution of Eq. (23) is

$$\nu(x,y) = A\cosh(\theta_1 y) + B\sinh(\theta_1 y) + C\cosh(\theta_2 y) + D\sinh(\theta_2 y). \tag{24}$$

Here $A(x), B(x), C(x)$ and $D(x)$ are the constants of integration, and θ_1 and θ_2 can be defined by

$$\theta_1 = \frac{1}{\sqrt{2}}\sqrt{((1-N)H^2\alpha + m^2) + \sqrt{((1-N)H^2\alpha + m^2)^2 - 4\left(\frac{2m^2(1-N)H^2\alpha}{(2-N)}\right)}}, \tag{25}$$

$$\theta_2 = \frac{1}{\sqrt{2}}\sqrt{((1-N)H^2\alpha + m^2) - \sqrt{((1-N)H^2\alpha + m^2)^2 - 4\left(\frac{2m^2(1-N)H^2\alpha}{(2-N)}\right)}}. \tag{26}$$

Substituting Eq. (23) into Eq. (21), we obtain

$$u = \frac{\xi(A\sinh(\theta_1 y) + B\cosh(\theta_1 y)) + \Omega(C\sinh(\theta_1 y) + D\cosh(\theta_2 y)) - (1-N)\frac{\partial p}{\partial x}}{(1-N)H^2\alpha}, \tag{27}$$

where ξ and Ω are defined by

$$\xi = (2-N)\theta_1\left(\frac{\theta_1^2}{m^2} - 1\right), \tag{28}$$

$$\Omega = (2-N)\theta_2\left(\frac{\theta_2^2}{m^2} - 1\right). \tag{29}$$

By using the boundary conditions, we get

$$u=\frac{-\frac{\partial p}{\partial x}}{H^2}\Big\{\frac{(\theta_2^2-m^2)\theta_2\tanh(\theta_1 h)(\frac{\cosh(\theta_2 y)}{\cosh(\theta_2 h)})+(m^2-\theta_1^2)\theta_1\tanh(\theta_2 h)(\frac{\cosh(\theta_1 y)}{\cosh(\theta_1 h)})}{(m^2-\theta_2^2)\theta_2\tanh(\theta_1 h)+(\theta_1^2-m^2)\theta_1\tanh(\theta_2 h)}-1\Big\}, \quad (30)$$

$$\nu=\frac{(1-N)m^2\frac{\partial p}{\partial x}\{\tanh(\theta_2 h)(\frac{\sinh(\theta_1 y)}{\cosh(\theta_1 h)})-\tanh(\theta_1 h)(\frac{\sinh(\theta_2 y)}{\cosh(\theta_2 h)})\}}{(2-N)\{(m^2-\theta_2^2)\theta_2\tanh(\theta_1 h)+(\theta_1^2-m^2)\theta_1\tanh(\theta_2 h)\}}. \quad (31)$$

We can find the corresponding stream function by using $u=\frac{\partial \psi}{\partial y}$ and $\psi=0$ at $y=0$,

$$\psi=\frac{-\frac{\partial p}{\partial x}}{H^2}\Big\{\frac{(\theta_1^2-m^2)\tanh(\theta_2 h)(\frac{\sinh(\theta_1 y)}{\cosh(\theta_1 h)})+(m^2-\theta_2^2)\tanh(\theta_1 h)(\frac{\sinh(\theta_2 y)}{\cosh(\theta_2 h)})}{(\theta_2^2-m^2)\theta_2\tanh(\theta_1 h)+(m^2-\theta_1^2)\theta_1\tanh(\theta_2 h)}-y\Big\}. \quad (32)$$

In the limit $N\to 0$, $m\to 0$, Eqs. (30–32) reduce to the classical Poiseuille MHD flow,

$$u=\frac{-\frac{\partial p}{\partial x}}{H^2\alpha}\Big\{\frac{\cosh(H\alpha y)}{\cosh(H\alpha h)}-1\Big\}, \quad \nu=0, \quad \psi=\frac{-\frac{\partial p}{\partial x}}{H^3\alpha}\Big\{\frac{\sinh(H\alpha y)}{\cosh(H\alpha h)}-H\alpha y\Big\}. \quad (33)$$

We can find the volume rate $Q(x)$ by

$$Q(x)=\int_0^h u(x,y)dy, \quad (34)$$

$$Q=\frac{\partial p}{\partial x}\Big\{\frac{(m^2-\theta_2^2)\sinh(\theta_1 h)(h\theta_2\cosh(\theta_2 h)-\sinh(\theta_2 h))}{H^2\{(\theta_2^2-m^2)\theta_2\cosh(\theta_2 h)\sinh(\theta_1 h)+(m^2-\theta_1^2)\theta_1\cosh(\theta_1 h)\sinh(\theta_2 h)\}}$$
$$+\frac{(\theta_1^2-m^2)\sinh(\theta_2 h)(h\theta_1\cosh(\theta_1 h)-\sinh(\theta_1 h))}{H^2\{(\theta_2^2-m^2)\theta_2\cosh(\theta_2 h)\sinh(\theta_1 h)+(m^2-\theta_1^2)\theta_1\cosh(\theta_1 h)\sinh(\theta_2 h)\}}\Big\}. \quad (35)$$

We can write Eq. (35) in the form

$$Q=-\frac{\partial p}{\partial x}\frac{1}{F(x)}, \quad (36)$$

where

$$F(x)=\frac{H^2\{(m^2-\theta_2^2)\theta_2\cosh(\theta_2 h)\sinh(\theta_1 h)+(\theta_1^2-m^2)\theta_1\cosh(\theta_1 h)\sinh(\theta_2 h)\}}{(m^2-\theta_2^2)\sinh(\theta_1 h)(h\theta_2\cosh(\theta_2 h)-\sinh(\theta_2 h))+(\theta_1^2-m^2)\sinh(\theta_2 h)(h\theta_1\cosh(\theta_1 h)-\sinh(\theta_1 h))}. \quad (37)$$

The pressure drop Δp ($=p$ at $x=0$, $-p$ at $x=L$) across the stenosis between the sections $x=0$ and $x=L$ is obtained from Eq. (36) as

$$\Delta p=\int_0^L\left(\frac{-dp}{dx}\right)dx=Q\int_0^L F(x)dx. \quad (38)$$

3 Resistance impedance and wall shear stress expression

3.1 Resistance impedance

The resistance to flow (resistance impedance) is obtained from Eq. (38) as

$$\lambda=\frac{\Delta p}{Q}=\Big\{\int_0^a F(x)|_{h=1}dx+\int_a^{a+b}F(x)dx+\int_{a+b}^L F(x)|_{h=1}dx\Big\}. \quad (39)$$

Thereby the resistance impedance is

$$\lambda = \{(L-b)I + \int_a^{a+b} F(x)dx\}, \tag{40}$$

where

$$I = \frac{H^2\{(m^2-\theta_2^2)\theta_2\cosh(\theta_2)\sinh(\theta_1) + (\theta_1^2-m^2)\theta_1\cosh(\theta_1)\sinh(\theta_2)\}}{(m^2-\theta_2^2)\sinh(\theta_1)(\theta_2\cosh(\theta_2)-\sinh(\theta_2)) + (\theta_1^2-m^2)\sinh(\theta_2)(\theta_1\cosh(\theta_1)-\sinh(\theta_1))}. \tag{41}$$

3.2 Wall shear stress

The nonzero shear stresses in our problem are given by

$$\tau_{xy} = 2\mu\frac{\partial u}{\partial y} - k\nu, \quad \tau_{yx} = (2\mu+\kappa)\frac{\partial u}{\partial y} + \kappa\nu. \tag{42}$$

By using Eq. (14) and letting $\tau' = \frac{d_0\tau}{2\mu u_0}$, we can find the dimensionalless nonzero shear stresses by

$$\tau_{xy} = \frac{\partial u}{\partial y} - \frac{N}{2(1-N)}\nu, \quad \tau_{yx} = \frac{1}{(1-N)}\left(\frac{\partial u}{\partial y} + \frac{N}{2}\nu\right). \tag{43}$$

From the second one of Eq. (43), we can find the expression for the wall shear stress by

$$\tau_{yx} = \frac{1}{(1-N)}\frac{\partial u}{\partial y}|_{r=h}, \tag{44}$$

where $\nu = 0$ at $y = h$. By using Eq. (30), we can find

$$\tau_{yx} = \frac{-\frac{\partial p}{\partial x}\{(\theta_1^2-\theta_2^2)(\theta_1^2+\theta_2^2-m^2)\}}{(1-N)H^2\alpha\{(m^2-\theta_2^2)\theta_2\coth(\theta_2 h) + (\theta_1^2-m^2)\theta_1\coth(\theta_1 h)\}}, \tag{45}$$

and from Eq. (36), we get

$$\tau_{yx} = \frac{Q(\theta_1^2-\theta_2^2)(\theta_1^2+\theta_2^2-m^2)}{(1-N)h\{(m^2-\theta_2^2)\theta_2\coth(\theta_2 h) + (\theta_1^2-m^2)\theta_1\coth(\theta_1 h) + (\theta_2^2-\theta_1^2)\}}. \tag{46}$$

The shearing stress at the stenosis throat (i.e., the wall shear at the maximum height of the stenosis located at $x = \frac{a}{b} + \frac{1}{n^{1/(n-1)}}$) is $\tau_{\rm s} = \tau_{yx}|_{h=1-\delta^*}$, and will take the form

$$\tau_s = \frac{Q(\theta_1^2-\theta_2^2)(\theta_1^2+\theta_2^2-m^2)}{(1-N)(1-\delta^*)\{(m^2-\theta_2^2)\theta_2\coth(\theta_2(1-\delta^*)) + (\theta_1^2-m^2)\theta_1\coth(\theta_1(1-\delta^*)) + (\theta_2^2-\theta_1^2)\}}, \tag{47}$$

We can find the final expressions for the dimensionless resistance to $\bar{\lambda}$, the wall shear stress $\bar{\tau}_{yx}$ and the shearing stress at the throat $\bar{\tau}_{\rm s}$ by

$$\bar{\lambda} = (1-\frac{b}{L})I + \frac{1}{L}\int_a^{a+b} F(x)dx, \tag{48}$$

$$\bar{\tau}_{yx} = \frac{(\theta_1^2-\theta_2^2)(\theta_1^2+\theta_2^2-m^2)}{(1-N)h\{(m^2-\theta_2^2)\theta_2\coth(\theta_2 h) + (\theta_1^2-m^2)\theta_1\coth(\theta_1 h) + (\theta_2^2-\theta_1^2)\}}, \tag{49}$$

$$\bar{\tau}_{\rm s} = \frac{(\theta_1^2-\theta_2^2)(\theta_1^2+\theta_2^2-m^2)}{(1-N)(1-\delta^*)\{(m^2-\theta_2^2)\theta_2\coth(\theta_2(1-\delta^*)) + (\theta_1^2-m^2)\theta_1\coth(\theta_1(1-\delta^*)) + (\theta_2^2-\theta_1^2)\}}, \tag{50}$$

where

$$\bar{\lambda} = \frac{\lambda}{\lambda_0}, \quad \bar{\tau}_{yx} = \frac{\tau_{yx}}{\tau_0}, \quad \bar{\tau}_{\rm s} = \frac{\tau_{\rm s}}{\tau_0}, \quad \lambda_0 = L, \quad \tau_0 = Q,$$

here λ_0 and τ_0 are the resistance to flow and the wall shear stress for a flow in a normal artery (no stenosis), respectively.

In the limit $B_0 \to 0$, $N \to 0$ and $m \to 0$, Eqs. (48)–(50) reduce to the same results as derived by Srivastava and Saxena[16] for the case of a Newtonian fluid model in the absence of a peripheral layer (i.e., $\alpha = 1$) and the particle phase in the core region (i.e., C=0), which further reduce to the case of a symmetric stenosis when $n = 2$ and correspond to the results obtained in the analysis of Young[24] as

$$\bar{\lambda} = (1 - \frac{b}{L})I + \frac{1}{L}\int_a^{a+b} \frac{dx}{h(x)^4}, \quad \bar{\tau}_{yx} = -\frac{1}{h(x)^3}, \quad \bar{\tau}_{\rm s} = -\frac{1}{(1-\delta^*)^3}. \tag{51}$$

4 Discussion of the results

To observe the quantitative effects of the Hartmann number H, the Hall parameter s, the length of the channel L and the shape parameter n, computer codes are developed for the numerical evaluations of the analytic results obtained for $\bar{\lambda}$, $\bar{\tau}_{yx}$ and $\bar{\tau}_{\rm s}$ (Eqs. (48)–(50)) for the values of parameters $\phi = 0$, $b = 1$, $L = 1$, 2, 10, $H = 1.5$, 2, 2.1, 2.2, 2.5, 3, 4, 5, $s = 0.5$, 1, 1.5, 2 and $n = 2$, 6, 11. The variations of the dimensionless resistance to flow, $\bar{\lambda}$, with δ^* for various values of the Hartmann number H, the Hall parameter s, the length of the channel L and the shape parameter n, are shown in Figs. 2–5. The wall shear stress distribution $\bar{\tau}_{yx}$ in the stenotic region for different values of H, s and the shape parameter n are displayed in Figs. 6–7. Whereas Figs. 8–9 represent the variations in the shearing stress at the stenosis throat $\bar{\tau}_{\rm s}$ with δ^* for different values of H and s; the variations of dimensionless resistance to flow, $\bar{\lambda}$, with the coupling parameter N and the micropolar parameter m for different values of the Hartmann number H and the Hall parameter s, are displayed in Figs. 10–11. Also, the wall shear stress distribution $\bar{\tau}_{yx}$ in the stenotic region for different values of M and N is displayed in Figs. 12–13. Finally, the effects of the Hartmann number H and the Hall parameter s on the horizontal velocity profile u of the fluid are displayed in Figs. 14–15.

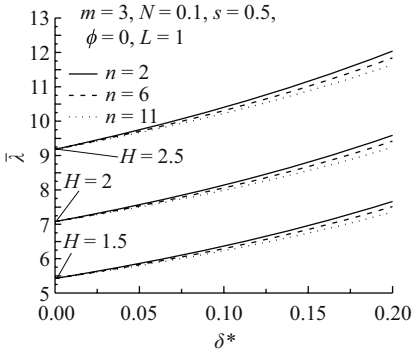

Fig. 2 Variation of dimensionless resistance to flow, $\bar{\lambda}$, with the ratio of the maximum height of the stenosis to the width of the channel δ^* for different values of the Hartmann number H and the shape parameter n

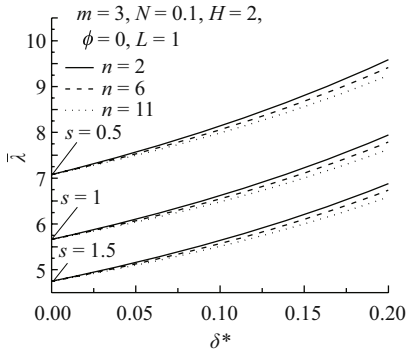

Fig. 3 Variation of dimensionless resistance to flow, $\bar{\lambda}$, with the ratio of the maximum height of the stenosis to the width of the channel δ^* for different values of the Hall parameter s and the shape parameter n

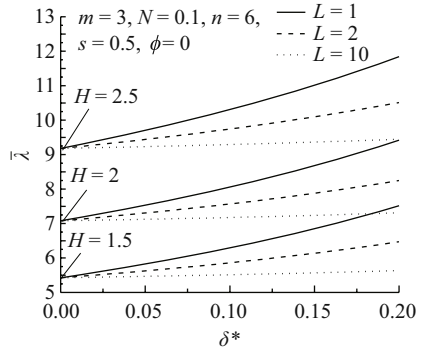

Fig. 4 Variation of dimensionless resistance to flow, $\bar{\lambda}$, with the ratio of the maximum height of the stenosis to the width of the channel δ^* for different values of the Hartmann number H and the length of the channel L

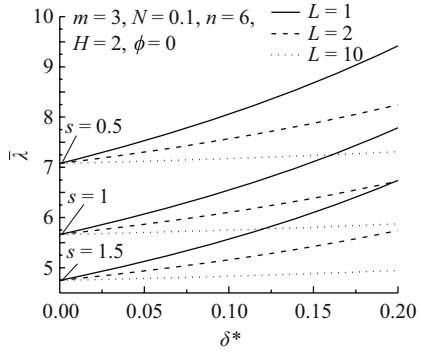

Fig. 5 Variation of dimensionless resistance to flow, $\bar{\lambda}$, with the ratio of the maximum height of the stenosis to the width of the channel δ^* for different values of the Hall parameter s and the length of the channel L

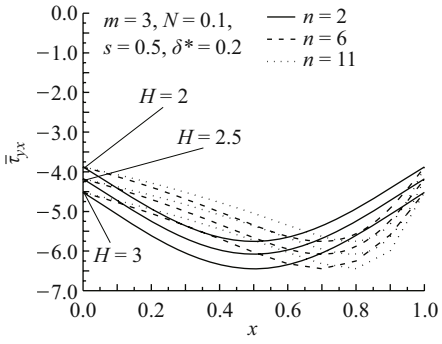

Fig. 6 Dimensionless wall shear stress, $\bar{\tau}_{yx}$, distribution in the stenotic region for different values of the Hartmann number H and the shape parameter n

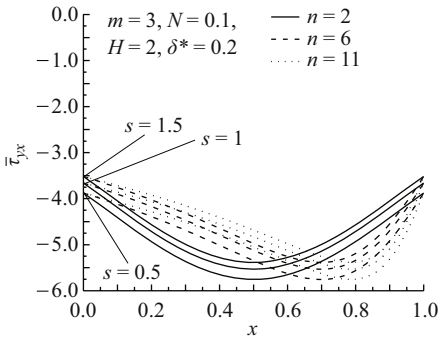

Fig. 7 Dimensionless wall shear stress, $\bar{\tau}_{yx}$, distribution in the stenotic region for different values of the Hall parameter s and the shape parameter n

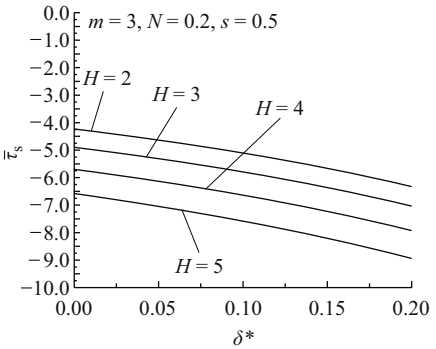

Fig. 8 Variation of the dimensionless shearing stress at the stenosis throat, $\bar{\tau}_{\rm s}$, with the ratio of the maximum height of the stenosis to the width of the channel δ^* for different values of the Hartmann number H

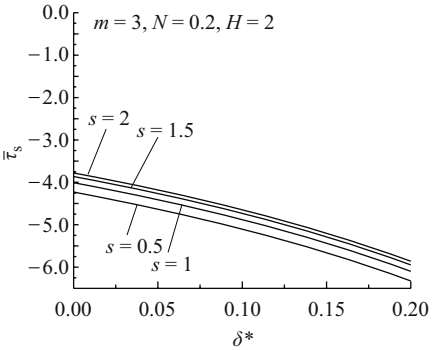

Fig. 9 Variation of the dimensionless shearing stress at the stenosis throat, $\bar{\tau}_{\rm s}$, with the ratio of the maximum height of the stenosis to the width of the channel δ^* for different values of the Hall parameter s

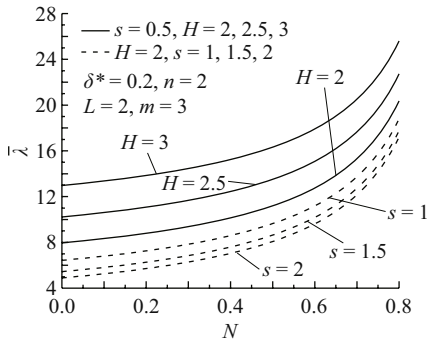

Fig. 10 Variation of dimensionless resistance to flow, $\bar{\lambda}$, with the coupling number N for different values of the Hartmann number H and Hall parameter s

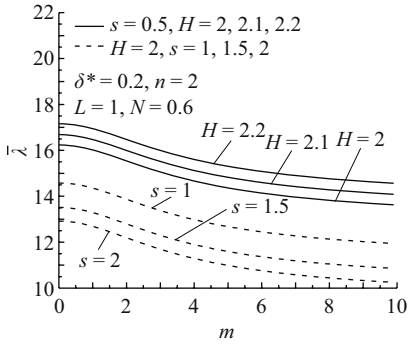

Fig. 11 Variation of dimensionless resistance to flow, $\bar{\lambda}$, with the micropolar number m for different values of the Hartmann number H and Hall parameter s

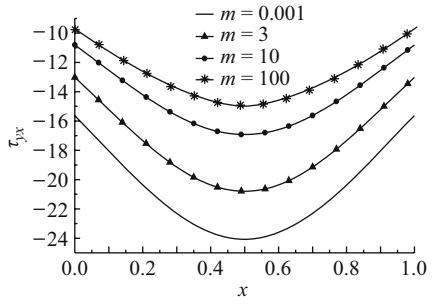

Fig. 12 Dimensionless wall shear stress, $\bar{\tau}_{yx}$, distribution in the stenotic region at $N = 0.8$, $n = 2$, $\delta^* = 0.2$, $H = 2$, $s = 0.5$ and for different values of the miropolar parameter m

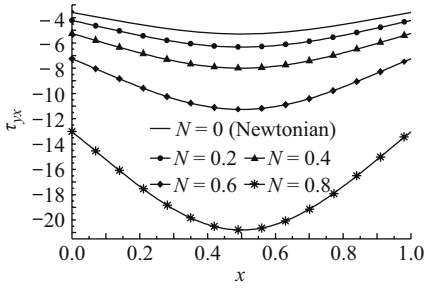

Fig. 13 Dimensionless wall shear stress, $\bar{\tau}_{yx}$, distribution in the stenotic region at $m = 3$, $n = 2$, $\delta^* = 0.2$, $H = 2$, $s = 0.5$ and for different values of the coupling number N

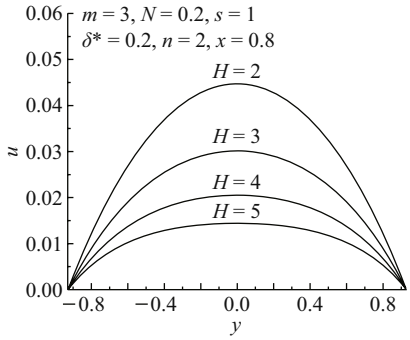

Fig. 14 Variation of velocity u with y for different values of the Hartmann number H

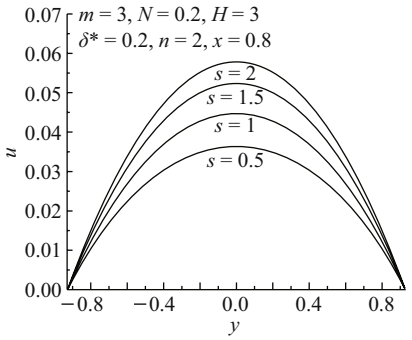

Fig. 15 Variation of velocity u with y for different values of the Hall parameter s

In Figs. 2–5, we observe that the resistance to flow $\bar{\lambda}$ increases with increasing Hartmann number H and stenosis size δ^*, while decreases with increasing the Hall parameter s, stenosis length L and the shape parameter n, and attains its maximum in the symmetric stenosis case, i.e., $n = 2$.

In Figs. 6–7, we notice that the wall shear stress distribution $\bar{\tau}_{yx}$ increases in the converging zone as the shape parameter n increases, while decreases in the diverging zone in a similar situation. For any given stenosis shape, the wall shear stress $\bar{\tau}_{yx}$ steeply decreases upstream from its approached value (i.e., at $x = 0$) to the peak value at the throat ($\bar{\tau}_{yx} = \bar{\tau}_s$), and then increases downstream of the throat and assumes its approached magnitude at the end point of the constriction profile (i.e., at $x = 1$). The rate of decreases (with respect to the horizontal distance) of $\bar{\tau}_{yx}$ upstream of the throat decreases with the increasing values of n, whereas the rate of increases of the same one downstream of the throat increases with n.

The wall shear stress distribution $\bar{\tau}_{yx}$ and its value at the throat $\bar{\tau}_{\rm s}$ possess inverse variations to the flow resistance $\bar{\lambda}$ with respect to the Hartmann number H and the Hall parameter s. $\bar{\tau}_{\rm s}$ is independent of the shape, and thus assumes the same magnitude for any value of n, see Figs. 6–9.

In Figs. 10–11, we study the variation of resistance to flow $\bar{\lambda}$ with the coupling parameter N and the micropolar parameter m for different values of H and s. We observe that the resistance to flow $\bar{\lambda}$ increases with increasing coupling parameter N (the particle size increases) and the Hartmann number H, while decreases with increasing micropolar parameter m (micropolar spin parameter increases) and the Hall parameter s. Also, from Figs. 12–13, we can see that the wall shear stress increases with the micropolar parameter M while decreases with the coupling number N.

Finally, the effect of H and s on the velocity profile of the fluid u is displayed in Figs. 14–15, where the velocity u decreases as H increases, and increases as s increases.

5 Concluding remarks

This problem is concerned with the analysis of a micropolar model for the blood simulating magnetohydrodynamic flow through a horizontally nonsymmetreic but vertically symmetric artery with a mild stenosis. Closed form analytic solutions are constructed for the axial velocity, the axial pressure gradient and the stream function. The expressions for the resistance impedance, the wall shear stresses in the stenotic region, and its magnitude at the maximum height of the stenosis (stenosis throat) are also given. The effect of various emerging parameters on the resistance impedance, wall shear stress distribution, shearing stresses at the throat and the axial velocity are shown with the help of graphs. From the presented analysis, the following conclusions can be drawn:

• The resistance to flow decreases with increasing values of the parameter determining the stenosis shape n and the stenosis length L, while increases with increasing the stenosis size δ^*.

• For a micropolar fluid, the resistance to flow increases with the coupling parameter N (particle size effect) and decreases with the micropolar parameter m (micropolar spin parameter effect).

• The magnitudes of the resistance to flow are higher in the case of a micropolar fluid model than in the case of a Newtonian fluid model.

• The magnitudes of the resistance to flow ($\bar{\lambda}$) are higher in the case of a magneto-micropolar fluid than in the case of a micropolar fluid.

• The wall shear stress and the shearing stress on the wall at the maximum height of the stenosis possess an inverse characteristic to the resistance to flow with respect to any given values of the Hartmann number H and the Hall parameter s.

• The axial velocity u increases as the Hall parameter s increases, and decreases as the Hartmann number H increases.

• The results in Ref. [16], $\alpha = 1$, $C = 0$, can be recovered by choosing $N \to 0, m \to 0$ and $B_0 \to 0$; and the results in Ref. [24] have been recovered by taking $N \to 0, m \to 0$ and $B_0 \to 0$ with $n = 2$.

References

[1] Craig I J D, Watson P G. Magnetic reconnection solutions based on a generalized Ohm's law[J]. *Solar Phys*, 2003, **214**(1):131–150.

[2] Stud V K, Sephon G S, Mishra R K. Pumping action on blood flow by a magnetic field[J]. *Bull Math Biol*, 1977, **39**:385-390.

[3] Agrawal H L, Anwaruddin B. Peristaltic flow of blood in a branch[J]. *Ranchi Univ Math J*, 1984, **15**:111-121.

[4] Bharali A, Borkakati A K. The effect of Hall currents on MHD flow and heat transfer between two parallel porous plates[J]. *Appl Sci Res*, 1982, **39**(2):155–165.

[5] Asghar S, Parveen S, Hanif S, Siddiqui A M, Hayat T. Hall effects on the unsteady hydromagnetic flows of an Oldroyd-B fluid[J]. *Int J Eng Sci*, 2003, **41**(6):609–619.

[6] Megahed A A, Komy S R, Afify A A. Similarity analysis in magnetohydrodynamics: Hall effects on free convection flow and mass transfer past a semi-infinite vertical flat plate[J]. *Non-Linear Mech*, 2003, **38**(4):513–520.

[7] Mohyuddin M R, Ashraf E E. Inverse solutions for a second-grade fluid for porous medium channel and Hall current effects[J]. *Proc Indian Acad Sci* (*Math Sci*), 2004, **114**(1):79–96.

[8] Hayat T, Naz R, Asghar S. Hall effects on unsteady duct flow of a non-Newtonian fluid in a porous medium[J]. *Appl Math Comp*, 2004, **57**(1):103–114.

[9] Hayat T, Wang Y, Hutter K. Hall effects on the unsteady hydromagnetic oscillatory flow of a second-grade fluid[J]. *Non-Linear Mech*, 2004, **39**(6):1027–1037.

[10] Eringen A C. Theory of micropolar fluids[J]. *J Math Mech*, 1966, **16**:11.

[11] Agarwal R S, Dhanapal C. Numerical solution to the flow of a micropolar fluid between porous walls of different permeability[J]. *Int J Eng Sci*, 1987, **25**:325–336.

[12] Haldar K. Effects of the shape of stenosis on the resistance to blood flow through an artery[J]. *Bull Math Biol*, 1985, **47**(4):545–550.

[13] Srivistava L M. Flow of couple stress fluid through stenotic blood vessels[J]. *J Biomech*, 1985, **18**(7):479–485.

[14] Srivastava V P. Arterial blood flow through a nonsymmetrical stenosis with applications[J]. *Jpn J Appl Phys*, 1995, **34**(12A):6539–6545.

[15] Ang K C, Mazumdar J N. Mathematical modeling of three dimensional flow through an asymmetric arterial stenosis[J]. *Math Comp Modelling*, 1997, **25**(1):19–29.

[16] Srivastava V P, Saxena M. Suspension model for blood flow through stenotic arteries with a cell-free plasma layer[J]. *Math Biosci*, 1997, **39**:79–102.

[17] Chakravarty S, Mandal P K. Two-dimentional blood flow through tapered arteries under stenotic conditions[J]. *Int J Non-Linear Mech*, 2000, **35**:779–793.

[18] Liu B, Tang D. A numerical simulation of viscous flows in collapsible tubes with stenosis[J]. *Appl Numer Math*, 2000, **32**(1):87–101.

[19] El-Shahed M. Pulsatile flow of blood through a stenosed porous medium under periodic body acceleration[J]. *Appl Math Comp*, 2003, **138**(2/3):479–488.

[20] Jung H, Choi J W, Park C G. Asymmetric flows of non-Newtonian fluids in symmetric stenosed artery[J]. *Korea-Australia Rheology Journal*, 2004, **16**(2):101–108.

[21] Liu G T, Wang X J, Ai B Q, Liu L G. Numerical study of pulsating flow through a tapered artery with stenosis[J]. *Chin J Phys*, 2004, **42**(4-I):401–409.

[22] Mandal P K. An unsteady of non-Newtonian blood flow through tapered arteries with a stenosis[J]. *Int J Nonlinear Mech*, 2004, **40**:151–164.

[23] Pralhad R N, Schulz D H. Modeling of arterial stenosis and its applications to blood diseases[J]. *Math Biosci*, 2004, **190**(2):203–220.

[24] Young D F. Effect of a time dependent stenosis of flow through a tube[J]. *J Eng Ind*, 1968, **90**:248–254.